RSC Advances

PAPER

View Article Online
View Journal | View Issue

Cite this: *RSC Adv.*, 2020, **10**, 20445

A novel biocompatible, simvastatin-loaded, bone-targeting lipid nanocarrier for treating osteoporosis more effectively†

Shan Tao,[a] Shao-qing Chen,[a] Wen-tao Zhou,[a] Fang-ying Yu,[a] Lu Bao,[a] Guo-xi Qiu,[a] Qing Qiao,[b] Fu-qiang Hu,[a] Jian-wei Wang*[c] and Hong Yuan*[a]

An insufficient drug concentration at the target site and drug efflux resulting in poor efficacy are recognized as important obstacles in osteoporosis treatment. Simvastatin (SIM), which can treat osteoporosis by promoting osteoblast differentiation and mineralization through the bone morphogenetic proteins (BMP)-Smad signaling pathway, has lower bioavailability, and less bone tissue distribution. Herein, novel lipid nanoparticles (LNPs) delivering SIM (SIM/LNPs) for osteoporosis therapy were developed with aspartic oligopeptide (ASP_n, here ASP_6)-based bone-targeting moieties grafted to the nanoparticles (SIM/ASP_6-LNPs) in an attempt to increase the concentration of SIM in bones with a relatively low dose to minimize adverse effects. *In vivo* experiments indicated that the ASP_6-LNPs exhibited ideal bone-targeting characteristics, and *in vitro* cell evaluation experiments showed LNPs have good biocompatibility with MC3T3-E1 cells. The cell mineralization experiment revealed that the SIM-loaded LNPs induced osteoblast differentiation and the formation of mineralized nodules in MC3T3-E1 cells, achieving the same efficacy as that of SIM. Pharmacodynamic experiments revealed that SIM/ASP_6-LNPs improved the efficacy of SIM on the recovery of bone mineral density when compared to SIM/LNPs or to SIM alone. Therefore, SIM/ASP_6-LNPs may represent a potential bone-targeting drug delivery system (DDS) that contributes to the development of a novel osteoporosis treatment.

Received 22nd January 2020
Accepted 11th May 2020

DOI: 10.1039/d0ra00685h

rsc.li/rsc-advances

1. Introduction

Bone is continuously rebuilt by osteoclasts removing old or damaged bone and by osteoblasts promoting the formation of new bone. The formation and resorption of bone is regulated by many factors. A slight imbalance among these factors can lead to skeletal system disease such as rheumatoid arthritis and osteoporosis.

Currently, osteoporosis is mainly treated with bisphosphonates, estrogen and related compounds, vitamin D analogs and calcitonin. Heo D. N. *et al.* reported that gold nanoparticles functionalized with cyclodextrin curcumin complexes could inhibit the differentiation of osteoclasts, which may be useful to prevent and treat osteoporosis.[1] In this regard, it was found that these therapies can only moderate the symptoms of osteoporosis, but cannot repair the damaged bone tissue.

Recent studies have revealed that SIM can increase the expression of BMP-2 in osteoblasts and promote the formation of new bone through the BMP-Smad signaling pathway. Mundy G. *et al.* reported that subcutaneous injection of SIM can promote bone formation, in addition to increasing the volume of rat cancellous bone when administered orally. Thus, statins may be applied for the treatment of osteoporosis.[2] Yamashita M. *et al.* reported that SIM can stimulate BMP-2 expression in osteoblasts, implicating the potential of SIM in promoting anabolic effects on bone.[3]

However, SIM degrades rapidly at a physiological pH, and its water solubility is poor, which leads to a low concentration at the bone site, which is not suitable for clinical application.[4] This low bioavailability may be the reason why a conventional dose of SIM is used clinically, the effects on bones are inconsistent.[5,6] To improve the water solubility, stability and bioavailability of SIM, a few SIM-based drug delivery systems (DDSs) have been proposed. Wang H. *et al.* reported a SIM-loaded tetracycline-grafted poly(lactic-*co*-glycolic acid) (PLGA) nanocarrier, which can transport SIM to bone sites to treat osteoporosis by promoting osteoblast differentiation and mineralization.[7] However, the size of the nanoparticles constructed by Wang H. *et al.* was relatively large, and the drug-loading efficacy was not high. In addition, tetracycline has certain side effects. Besides, most of SIM-based drug delivery systems (DDSs) are about the

[a]College of Pharmaceutical Sciences, Zhejiang University, 866 Yuhangtang Road, Hangzhou, 310058, China. E-mail: yuanhong70@zju.edu.cn; Tel: +86-136-06804049
[b]Anesthesia Department, Zhejiang University School of Medicine, Sir Run Run Shaw Hospital, 3 Qingchun East Road, Hangzhou, 310016, China
[c]Department of Orthopaedics, The Second Affiliated Hospital of Zhejiang University School of Medicine, 88 Jiefang Road, Hangzhou, 310009, China. E-mail: zjuwjw@zju.edu.cn; Fax: +86-571-87022776; Tel: +86-159-58185118

† Electronic supplementary information (ESI) available. See DOI: 10.1039/d0ra00685h

treatment of bone defects through put the scaffold at the bone defects site, which is not suitable to the treatment of osteoporosis. Zhang Z. *et al.* reported a 3D printed poly(ε-caprolactone) scaffolds function with SIM-loaded poly(lactic-*co*-glycolic acid) microspheres to repair load-bearing segmental bone defects.[8] Yu W. *et al.* demonstrated that the water-insoluble SIM could be incorporated into the mesoporous hydroxyapatite microspheres (MHMs) and maintained its biological activities, more importantly, the SIM-loaded MHMs (S-MHMs)/collagen scaffolds fabricated in this study are of immense potential in bone defect repair by enhancing osteogenesis and angiogenesis simultaneously.[9] In any case, these studies point to a new generation of osteoporosis treatments with SIM, breaking traditional methods of inhibiting osteoclast activity.

LNPs, which are based on lipid materials with good biocompatibility, have been extensively studied.[10,11] They are biocompatible and can effectively encapsulate drugs, with a high drug loading capacity. In addition, they can be made *via* large-scale production.[12,13] Hence, LNPs could be a promising vehicle to deliver SIM. Yue X. *et al.* reported a SIM-loaded nanostructured lipid carrier, which could be a potential encapsulation carrier system for SIM in bone regeneration applications.[14] However, due to the special microenvironment of the bone site and the poor permeability of the bone tissue, effective accumulation of SIM at the bone site remains difficult. Therefore, we urgently need a bone-targeted modification to target LNPs to bones, thereby increasing the efficacy of SIM.

It has previously been reported that bone disease may produce local inflammation and/or lead to blood exposure of hydroxyapatite (HAP),[15] which opens up a path for bone targeting. Most of the current studies have used tetracycline and diphosphate as the bone-targeting groups. These compounds are able to adsorb to HAP in bone and show special affinity for bones.[15–17] Ye W. *et al.* synthesized a doxorubicin-poly(ethyleneglycol)-alendronate (DOX-hyd-PEG-ALN) micelle, which can accumulate more DOX in bone metastases, thereby greatly improving the anti-tumor ability of micelles and reducing systemic toxicity.[17] Wang H. *et al.* reported a SIM-loaded tetracycline-grafted poly(lactic-*co*-glycolic acid) (PLGA) nanocarrier, which is expected to treat osteoporosis with SIM.[7] However, bisphosphonates can induce hypocalcemia, nephrotoxicity, ocular dysfunction and osteonecrosis of the jaw. Tetracycline can dye teeth yellow and inhibit the growth of skeletal tissue in children. McClung M. *et al.* described the unexpected side effects of millions of patients after using bisphosphonates in clinical practice, including atypical femur fractures, osteonecrosis of the jaw, esophageal cancer and atrial fibrillation.[18] In addition, Vennila V. *et al.* reported that tetracycline can incorporate into active mineralization sites such as dental tissues and skeletal tissue and stain these tissues.[19] Therefore, the need to identify a new bone-targeting modality is urgently needed. It has been reported that many types of acidic oligopeptides (AOs), such as glutamic acids (Glu)*n*, aspartic acids (Asp)*n* and aspartic acids–serine–serine (Asp–Ser–Ser)*n*, can accumulate at bone sites after injection through the vein.[20,21] Carboxylic acids, such as Glu and Asp, have good biocompatibility, and they are rapidly degraded and removed from plasma. Therefore, they could be a promising bone-targeting modality. In addition, Murphy M. B. *et al.* reported that AOs can bind to HAP faster than bisphosphonate (BP) can.[22] This result may be caused by AOs, which have a larger binding area.[23] Sekido *et al.* analyzed

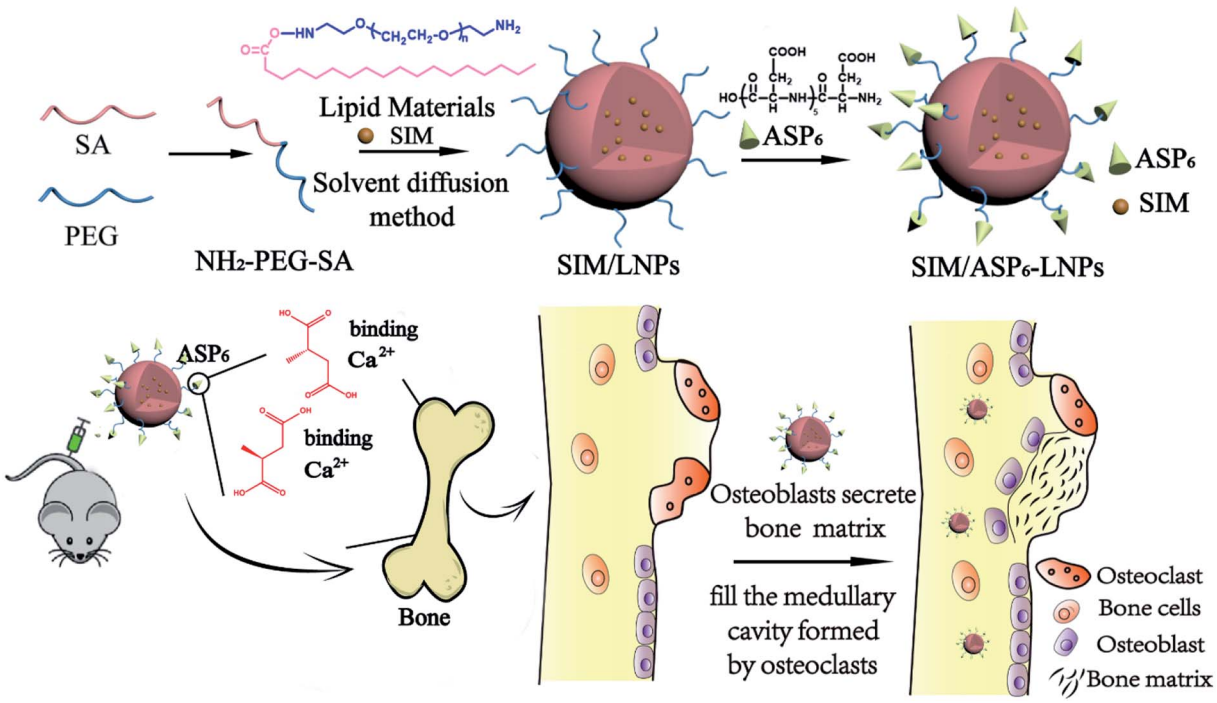

Fig. 1 A scheme of the preparation of SIM/ASP$_6$-LNPs and a mechanism which indicated that SIM/ASP$_6$-LNPs could improve the efficacy of SIM on the recovery of osteoporosis under the action of bone-targeting moieties ASP$_6$.

the binding rates of different chain lengths of $(Asp)_{2-10}$ to HAP.[24] The results showed that when the length of the ASP chain was less than 6, as the chain length increased, the binding rate increased, and ASP_6 had the highest binding rate; however, further increasing the chain length produced no effect on binding rates. The results suggested that ASP_6 is an excellent candidate for selective drug delivery to bone.

In view of the importance of the above studies, as displayed in Fig. 1, SIM-loaded lipid nanoparticles with ASP_6 grafted (SIM/ASP_6-LNPs) were prepared as a bone-targeting DDS for osteoporosis therapy. We studied the effect of SIM/ASP_6-LNPs *in vivo* and *in vitro*. The results revealed that the nanocarriers can promote targeted delivery of the anti-osteoporosis drug SIM, breaking traditional methods of inhibiting osteoclast activity and indicating to a new generation of treatments for osteoporosis.

2. Results and discussion

2.1 Synthesis and characterization of amino-terminated polyethylene glycol monostearate (NH_2-PEG_{2000}-SA)

A chemical binding method was used to conjugate ASP_6 to the nanocarriers. NH_2-PEG_{2000}-SA was synthesized first as an ingredient of the LNPs. Then, the ASP_6-LNPs were prepared by the conjugation between the amino groups of ASP_6 and the amino group of NH_2-PEG_{2000}-SA mediated by *N*,*N*′-disuccinimidyl carbonate (DSC). NH_2-PEG_{2000}-SA was synthesized *via* reaction between the carboxyl groups of stearic acid (SA) and the amine groups of amino-terminated polyethylene glycol (NH_2-PEG_{2000}-NH_2) under catalytic conditions of *N*-(3-dimethylaminopropyl)-*N*′-ethylcarbodiimide hydrochloride (EDC) and *N*-hydroxysuccinimide (NHS). Afterwards, ^{1}H NMR spectra and IR spectra (Fig. 2) demonstrated the successful synthesis of NH_2-PEG_{2000}-SA. The ^{1}H NMR spectra indicated that peaks at 0.96 ppm and 1 ppm corresponding to the $-CH_3$ and $-CH_2$ of SA, respectively, and the peak at 3.63 ppm represented the $-CH_2CH_2O-$ of NH_2-PEG_{2000}-NH_2. We observed all of the abovementioned peaks in addition to a peak at 12.09 ppm, which represents the carboxyl of SA, indicating that the carboxyl of SA had combined with the amino of NH_2-PEG_{2000}-NH_2. These results revealed that NH_2-PEG_{2000}-SA was successfully synthesized. Meanwhile, in the IR spectra, NH_2-PEG_{2000}-SA exhibited absorption bands at 1637 cm^{-1} (amide bond I), 1553 cm^{-1} (amide bond II) and 3311 cm^{-1} (amidogen), while absorption bands at 1703 cm^{-1} (carbonyl) and 2917 cm^{-1} (carboxyl) of SA were not observed. These results all indicate the successful formation of NH_2-PEG_{2000}-SA.

Besides, ^{1}C NMR spectra (Fig. S2†) and mass spectrum (Fig. S3†) were also performed to further demonstrated the successful synthesis of NH_2-PEG_{2000}-SA. From the ^{1}C NMR spectra, we could see that the chemical shift of the carboxyl carbon of SA decreases from 175.343 ppm to 173.165 ppm, indicating that the carboxyl group of SA has undergone an amide reaction. In NH_2-PEG_{2000}-SA, we also observed the $-CH_2$-O– of NH_2-PEG_{2000}-NH_2 (70.824 ppm and 70.828 ppm), indicating the successful synthesis of NH_2-PEG_{2000}-SA. Last but not least, from the mass spectrum, we can see that the molecular weight of SA is 283.2644, which is in line with the expected result (284); however, NH_2-PEG_{2000}-NH_2 is a polymer, so we could observe different molecular weights of NH_2-PEG-NH_2, which included NH_2-PEG_{2000}-NH_2 with a molecular weight of 1999.1755. When NH_2-PEG_{2000}-NH_2 has a reaction with SA, NH_2-PEG_{2000}-SA (molecular weights is 2266) and SA-PEG_{2000}-SA (molecular weights is 2532) could be generated, while in the NH_2-PEG_{2000}-SA spectrum, we only observed 2265.4158 and not observed 2532, indicating that we synthesized NH_2-PEG_{2000}-SA successfully.

2.2 Preparation and characterization of LNPs and ASP_6-LNPs

The blank LNPs and ASP_6-LNPs were prepared with a solvent diffusion method. The freeze-dried LNPs and Asp_6-LNPs were analyzed by an elemental analyzer. The N content of LNPs is mainly derived from PEG. However, after grafting ASP_6, the N of

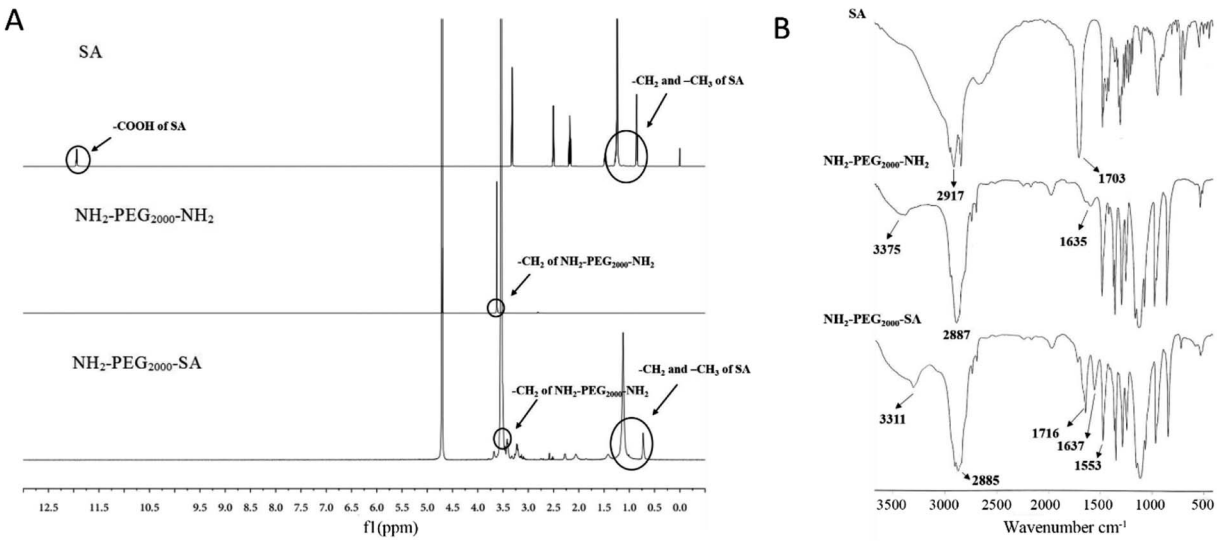

Fig. 2 Characterization of NH_2-PEG_{2000}-SA. (A) ^{1}H NMR spectra. (B) IR spectra. These results all indicate the successful formation of NH_2-PEG_{2000}-SA.

Table 1 Elemental analysis of LNPs and ASP_6-LNPs[a]

Carriers	Weight (mg)	N area	C area	H area	N (%)	C (%)	H (%)
LNPs	1.9780	55	29 201	14 918	0.09	69.68	10.68
ASP_6-LNPs	1.9770	126	28 724	15 654	0.20	68.57	11.22

[a] The N (%), C (%) and H (%) represent the element content of LNPs and ASP_6-LNPs, respectively.

Table 2 Physicochemical characterization of the LNPs[a]

Carriers	Size (nm)	PI	Zeta potential (mV)	DL (%)	EE (%)
LNPs	95.25 ± 0.40	0.14 ± 0.01	−25.70 ± 0.53	—	—
ASP_6-LNPs	121.63 ± 3.83	0.16 ± 0.01	−26.37 ± 0.12	—	—
SIM/LNPs	129.27 ± 5.95	0.19 ± 0.02	−20.37 ± 1.07	3.90 ± 0.10	97.50 ± 0.25
SIM/ASP_6-LNPs	154.30 ± 2.45	0.21 ± 0.01	−22.63 ± 0.50	3.89 ± 0.15	97.30 ± 0.57

[a] The PI, EE and DL represent the polydispersity index, drug encapsulation efficiency and drug loading content, respectively. The data represent the means ± SDs ($n = 3$).

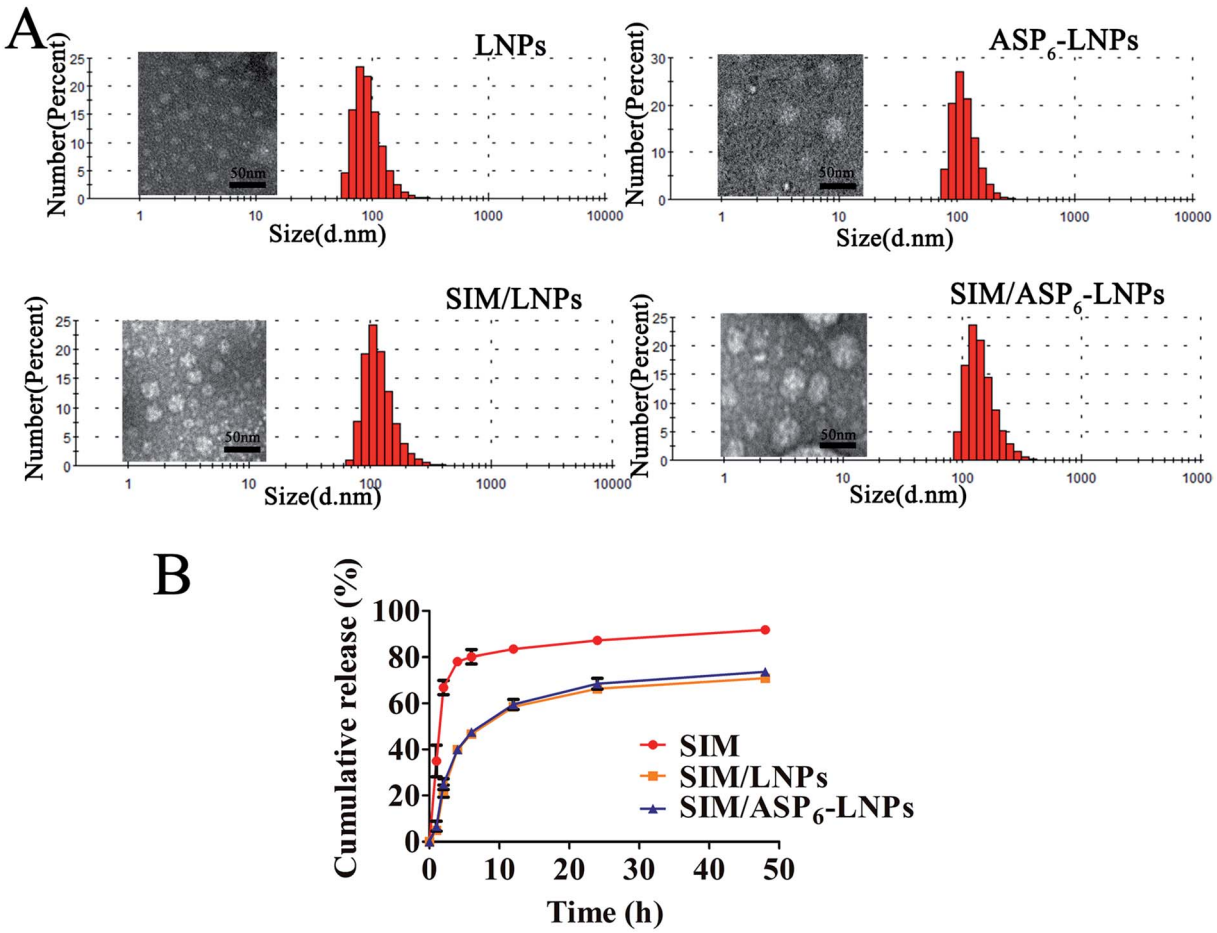

Fig. 3 Characterization of LNPs. (A) Morphology (left, TEM) and size distribution (right, DLS) of LNPs, ASP_6-LNPs, SIM/LNPs and SIM/ASP_6-LNPs, demonstrating the size of SIM-loaded LNPs are a little larger than blank LNPs due to the SIM contained in them. Scale bar: 100 nm. (B) *In vitro* release profiles of free SIM, SIM/LNPs and SIM/ASP_6-LNPs. A slower drug release is observed in SIM-loaded LNPs. The data represent the means ± SDs ($n = 3$).

ASP_6 will increase the N content of ASP_6-LNPs. As we can see, after ASP_6 grafting, the N content increased, from 0.09% to 0.2%, which meant that ASP_6 was grafted successfully (Table 1).

2.3 Characterization of blank LNPs and SIM-loaded LNPs (SIM/LNPs)

2.3.1 Size, zeta potential and morphology measurements. The size distribution and morphology of LNPs and SIM/LNPs were observed through dynamic light scattering (DLS) and transmission electron microscopy (TEM) images. Table 2 shows that the sizes of blank LNPs and SIM/LNPs were approximately 100 nm and the sizes of SIM-loaded LNPs are a little larger than blank LNPs due to the SIM contained in them. The polydispersity index (PI) of LNPs was approximately 0.2, and the zeta potential was approximately −25 mV. Fig. 3A shows the morphology of LNPs through transmission electron microscopy (TEM), from which we could see that the LNPs were spherical or spherical-like particles and were well dispersed. The DL% and EE% are shown in Table 2. The drug encapsulating efficiencies of SIM/LNPs and SIM/ASP_6-LNPs were 97.50 ± 0.25% and 97.30 ± 0.57%, respectively, and the drug loading efficiencies were 3.90 ± 0.10% and 3.89 ± 0.15%, respectively, when the concentration of SIM administered was 4%. These results indicate that LNPs can effectively encapsulate SIM, and the encapsulation of SIM is not affected before or after ASP_6 grafting.

2.3.2 *In vitro* SIM release from SIM/LNPs and SIM/ASP_6-LNPs. The *in vitro* drug release behaviors are shown in Fig. 3B. As we can see, more than 80% free SIM was released from the dialysis bag within 10 h, indicating that the dialysis bag did not hinder the release of the drug. The SIM/LNPs and SIM/ASP_6-LNPs exhibited a cumulative drug release of 70% over 48 h. Compared to free SIM, the slower drug release from SIM/LNPs and SIM/ASP_6-LNPs indicated that the nanocarrier could decrease the SIM leakage in the bloodstream, thereby increasing SIM accumulation in bones. In addition, the release results of the LNPs and ASP_6-LNPs were not significantly different, indicating that the ASP_6 graft did not affect the release results.

2.4 Cell culture and evaluation

2.4.1 Cytotoxicity. Fig. 4A shows the cytotoxicity of the LNPs and ASP_6-LNPs on MC3T3-E1 cells. The results showed that the 50% cellular growth inhibition (IC_{50}) values of LNPs and ASP_6-LNPs were 392 μg mL^{-1} and 475 μg mL^{-1}, respectively, which suggested that the nanocarriers had low cytotoxic effects on MC3T3-E1 cells. To determine the optimal concentration of SIM/LNPs for osteoblast differentiation and mineralization, we treated MC3T3-E1 cells with different concentrations of SIM/LNPs. Fig. 4B shows that SIM/LNPs reduced the toxic effect on MC3T3-E1 cells (a clonal pre-osteoblastic cell line derived from newborn mouse calvaria) and improved the biocompatibility of SIM compared to free SIM, especially when the concentration of SIM was higher than 1×10^{-6} mol L^{-1}. Meanwhile, there was no significant difference when comparing SIM/LNPs with SIM/ASP_6-LNPs in the cytotoxic effects on MC3T3-E1 cells, indicating that the grafting of ASP_6 had a negligible effect. In addition, when the concentration of SIM was higher than 5×10^{-7} mol L^{-1}, the cytotoxicity of the SIM and SIM/LNPs groups was significantly increased and the cell viability was decreased compared with

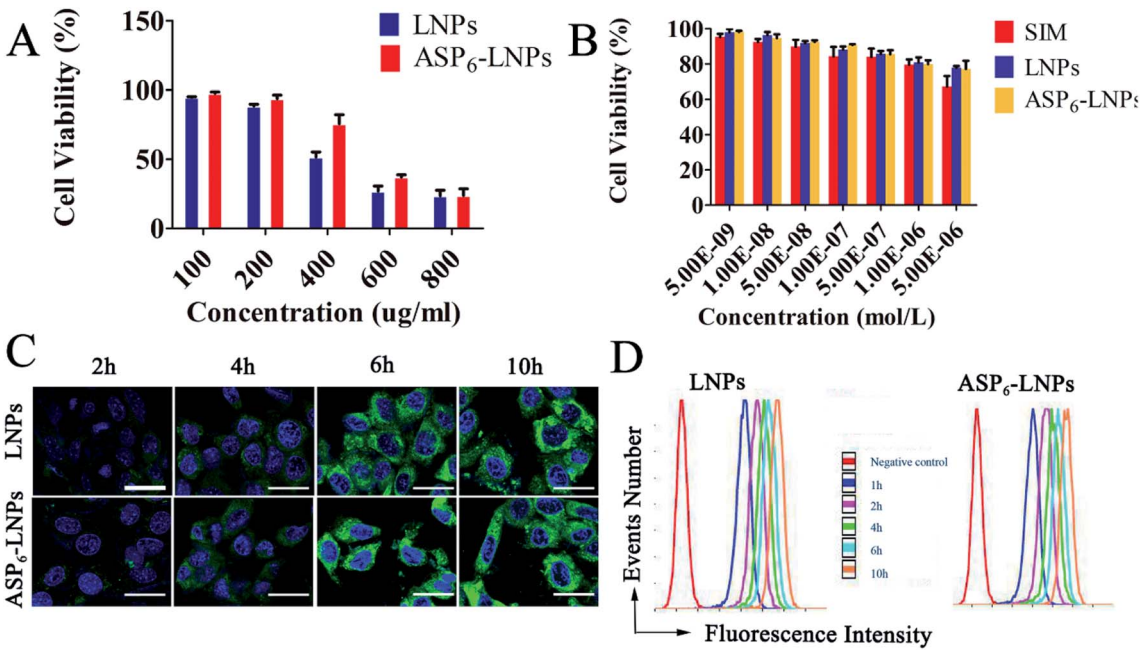

Fig. 4 The cytotoxicity and cellular uptake of LNPs in MC3T3-E1 cells. The cell viability influence of blank LNPs (A) and SIM/LNPs (B) on MC3T3-E1 cells after incubation for 48 h. (C) Cellular uptake in MC3T3-E1 cells incubated with ODA-FITC-labeled LNPs and ASP_6-LNPs for 2, 4, 6 and 8 h, respectively. Green: ODA-FITC labeled LNPs; blue: DAPI stained cell nucleus. Scale bar = 30 μm. (D) Semiquantitative analysis of cellular uptake by flow cytometry, demonstrating a time-dependent cell uptake behavior of LNPs.

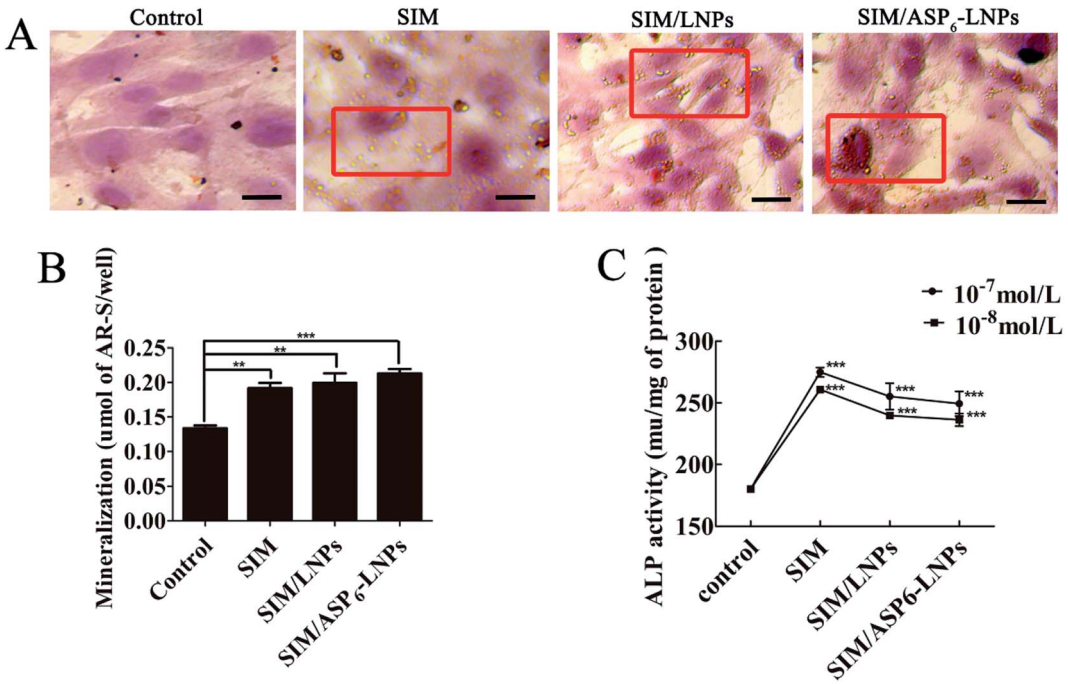

Fig. 5 Effects of SIM-loaded LNPs on mineralized nodule formation and ALP activity in MC3T3-E1 cells. Mineralized nodule of the extracellular matrix by optical microscopy and macroscopic observation. Inset red frame indicated increased mineralized nodule compared with the control (A), quantitative mineralization results (B), and stimulation of ALP activity by SIM (10^{-7} M and 10^{-8} M) (C). The results represent the means ± SDs (n = 3), *p < 0.05, **p < 0.01, ***p < 0.001, significant differences compared with the control. Scale bar = 30 μm.

the untreated control cells. Therefore, when we performed cell differentiation and mineralization experiments, the drug concentration was kept below 5×10^{-7} mol L^{-1}.

2.4.2 Cellular uptake study. Octadecylamine-fluorescein isothiocyanate (ODA-FITC) was used to label LNPs. 4′,6-Diamidino-2-phenylindole (DAPI) was used to stained cell nucleus blue. The green fluorescence signal represents ODA-FITC labeled LNPs, which was observed after 2 h of incubation (Fig. 4C). As the incubation time was prolonged, a gradual increase in the fluorescence signal was observed. The results showed that LNPs had good cell uptake behavior in a time-dependent manner. Therefore, LNPs can effectively deliver drugs to cells to achieve the desired function.[25] Meanwhile, semiquantitative analysis of cellular uptake revealed similar results (Fig. 4D).

2.4.3 Effects of SIM/LNPs on mineralized nodule formation. The interference of SIM/LNPs on osteoblast mineralization was assessed by quantitative mineralization experiments. First, MC3T3-E1 cells were cultured in osteogenic differentiation and mineralization medium for 14 days with SIM/LNPs and SIM/ASP_6-LNPs (equal SIM concentration: 10^{-7} M). The medium used in osteogenic differentiation and mineralization experiments contained 10 mM β-glycerophosphate and 50 μg mL^{-1} ascorbic acid, which is widely employed as the standard medium in osteogenic differentiation and mineralization experiments[26,27] and has been reported to possess osteogenic activities.[28] In view of the osteogenic effects of the osteogenic differentiation medium, differentiation medium without LNPs was used as the control treatment. As shown in Fig. 5A, the increased mineralized nodules (red frame) can be observed in the group cultured with free SIM when compared to the control group, and the difference was significant. This result is due to the potential of SIM to increase BMP-2 expression in osteoblasts and promote the differentiation and mineralization of osteoblasts through the BMP-Smad signaling pathway. Meanwhile, it is known from the release results that LNPs and ASP_6-LNPs can effectively release SIM. Therefore, we observed the same mineralized nodules in the SIM/LNP and SIM/ASP_6-LNP groups. However, there were no significant differences among the SIM, SIM/LNPs and SIM/ASP_6-LNPs groups in the formation of mineralized nodules when the concentrations were the same. In addition, quantitative analysis of alizarin red S staining is shown in Fig. 5B. The results showed that SIM/LNPs and SIM/ASP_6-LNPs can significantly promote the formation of MC3T3-E1 cell mineralization nodules and achieve similar effects to those of free SIM, indicating LNPs could be a promising vehicle to deliver SIM.

2.4.4 Effects of SIM-loaded LNPs on alkaline phosphatase (ALP) activity. SIM has the potential to increase BMP-2 expression and promote the formation of new bone *in vitro*. A marker of new bone formation is an increase in the activity of ALP, an enzyme serving as a marker during osteoblast differentiation. Therefore, we examined the expression of ALP in MC3T3-E1 cells treated with SIM/LNPs and SIM/ASP_6-LNPs (equal SIM concentration). The medium without SIM or LNPs was used as the control treatment. The result suggested that free SIM increases ALP activity and SIM-loaded LNPs (equal SIM concentrations: 10^{-7} M and 10^{-8} M) exert almost the same effect (Fig. 5C). Significant differences among all

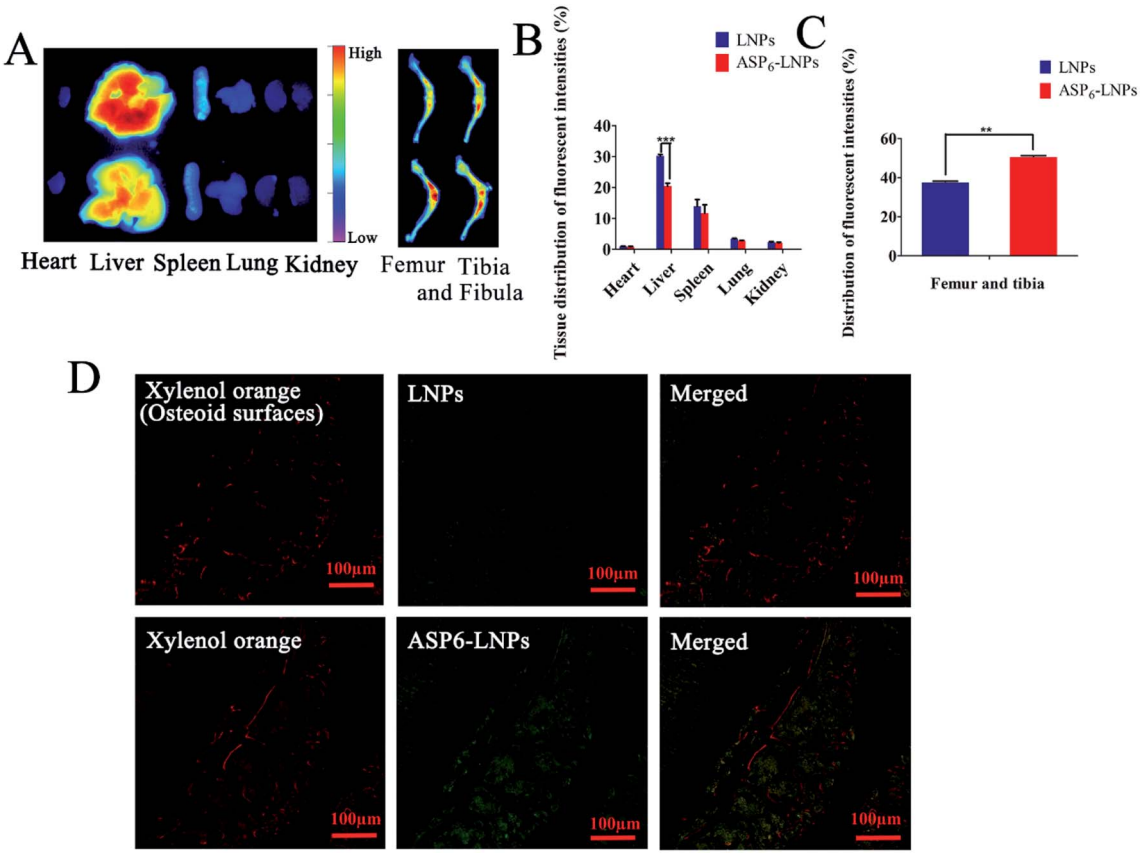

Fig. 6 *In vivo* distribution and intrabone distribution of LNPs and ASP_6-LNPs. (A) Fluorescence images of the major tissues (heart, liver, spleen, lung, kidney) and the femur and tibia bones after tail-intravenously injected with DiR-loaded LNPs and ASP_6-LNPs in ICR mice for 48 h. (B) Quantitative results of the major tissues. (C) Quantitative results of the femur, and tibia bones. (D) Intrabone distribution of ODA-FITC-labeled LNPs and ASP_6-LNPs in undecalcified frontal tissue sections from the distal femur and proximal tibia. Green: ODA-FITC labeled LNPs; red: xylenol orange stained the osteoid surface. The results represent the means ± SDs ($n = 3$), scale bar: 100 μm *$p < 0.05$, **$p < 0.01$, ***$p < 0.001$.

drug-administered groups and the control group were observed, indicating that the constructed nanocarrier has the potential to promote new bone formation.

2.5 *In vivo* test

2.5.1 *In vivo* distribution of LNPs and ASP_6-LNPs. As shown in Fig. 6A, the fluorescence signals are mainly concentrated on the liver and spleen, while there are fewer on other organs. This result is due to the important role that macrophages of the liver and spleen play in uptake and phagocytosis.[29] In addition, the fluorescence signals in the liver of the ASP_6-LNP-treated group were significantly reduced when compared to those of the LNP control group; meanwhile, the fluorescence intensities in the bone of the ASP_6-LNP group were obviously higher than those in the LNPs control group. This result was observed because compared with LNPs, ASP_6-LNPs have a bone-targeting group, ASP_6, which is hydrophilic. The modification of adding ASP_6 to LNPs increases the hydrophilicity of LNPs, allowing LNPs to escape the phagocytosis of mononuclear macrophages and prolong *in vivo* circulation time. During systemic circulation, ASP_6 can combine with the hydroxyapatite of the bone so that more ASP_6-LNPs can be distributed to the bone.

The fluorescence intensities were then quantified. As shown in Fig. 6B and C, 32.5% and 15.7% fewer (1,1′-dioctadecyl-3,3,3′,3′-tetramethylindotricarbocyanine iodide) DiR-loaded ASP_6-LNPs were detected in the liver and spleen than were DiR-loaded LNPs, respectively. However, there were 29.1% more DiR-loaded ASP_6-LNPs detected in the femur and tibia. The results showed that ASP_6-LNPs can reduce the capture of LNPs by the liver and spleen, thereby reducing the toxic side effects of LNPs on other organs. This may be an important piece of evidence that ASP_6-LNPs can target bone tissue and accumulate at bone sites. Therefore, the biodistribution results revealed the potential of ASP_6-LNPs for bone-targeted delivery.

2.5.2 Intrabone distribution of ODA-FITC-labeled LNPs and ASP_6-LNPs. The intrabone distribution of ODA-FITC-labeled LNPs and ASP_6-LNPs in the distal femur and proximal tibia is shown in Fig. 6D. As reported, xylenol orange can selectively accumulate on the osteoid surface.[30] Therefore, the osteoid surface of undecalcified tissue sections was stained red by xylenol orange. In addition, ODA-FITC-labeled LNPs were scarcely detected in the tissue sections. However, due to the bone targeting group ASP_6, ODA-FITC-labeled ASP_6-LNPs are distributed more in the bone, so they were clearly observed. These findings indicated

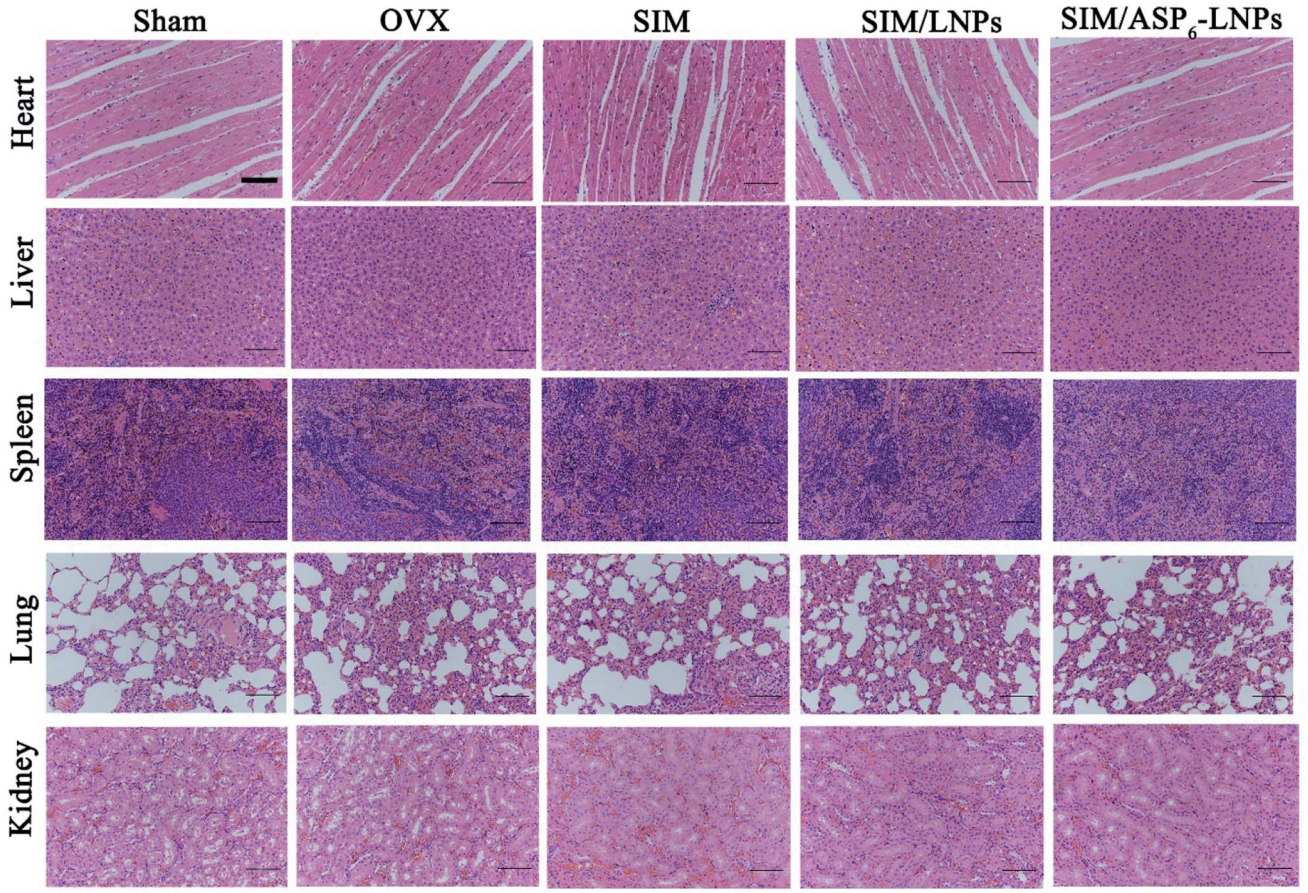

Fig. 7 Histological analysis of organs from all experimental groups. H&E staining of heart, liver, spleen, lung, kidney, indicating the carrier has good biocompatibility. Scale bar = 50 μm.

that ASP_6-LNPs can be used as a promising nanocarrier for the targeted treatment of bone diseases.

2.5.3 Animal pharmacodynamics study

2.5.3.1 Histological analysis of excised organ samples. Hematoxylin and eosin (H&E) staining of organs revealed that there were no significant pathological changes in organs, indicating that the carrier has good biocompatibility and the results are shown in Fig. 7.

2.5.3.2 Microcomputed tomography (micro-CT) and image analysis. Micro-CT scanning was used to analyze the trabecular bone mineral density (BMD), trabecular bone volume percentage (BV/TV), trabecular separation (Tb. Sp), trabecular thickness (Tb. Th) and trabecular number (Tb. N) at 12 weeks posttreatment (Fig. 8A). In Fig. 8A, the femur BMD is distinctly different between the Sham (the control sham-operated rats) group and the OVX (the ovariectomized rats) group, with a value of 0.186 ± 0.008 g cm^{-2} in the Sham group and 0.118 ± 0.002 g cm^{-2} in the OVX group. The BMD of the OVX group was reduced by 36.56% compared to that in the Sham group, indicating that the osteoporotic model rats were established successfully.

BMD and BV/TV are extensively used as predictors for evaluating osteoporosis. It was clearly observed that the BMD and BV/TV values of all treatment groups were significantly increased compared to those of the OVX group after 12 weeks (Fig. 8A). Meanwhile, all treatment groups showed a significant increase in Tb. Sp, Tb. Th and Tb. N when compared to the OVX group. However, we observed that the most trabecular bone tissue was observed in the SIM/ASP_6-LNPs group. This finding is because the modification of ASP_6 can increase the distribution of SIM/ASP_6-LNPs in bone, as shown by the *in vivo* distribution of LNPs and ASP_6-LNPs, thereby increasing the concentration of SIM at the bone site and increasing the efficacy of bone targeting. As we can see, the BMD and BV/TV of the SIM/ASP_6-LNPs group were 0.176 ± 0.013 and 42.204 ± 3.575, which were almost the same as the BMD and BV/TV of the SHAM group (0.186 ± 0.008 and 46.403 ± 3.494, respectively). These results indicated that LNPs could be a promising vehicle to deliver SIM, especially ASP_6-LNPs, which could best promote osteoblast differentiation and mineralization, thereby repairing damaged bone tissue. Almost all of the results consistently revealed that SIM/ASP_6-LNPs can increase bone density more than the other experimental treatments could. In addition, there was a statistically significant difference in all evaluation indicators between the SIM/ASP_6-LNPs groups and the other groups treated with supplements. 2D images and 3D images of trabecular bone (Fig. 8B) measured by micro-CT also revealed a significant difference between the treatment groups and the OVX group,

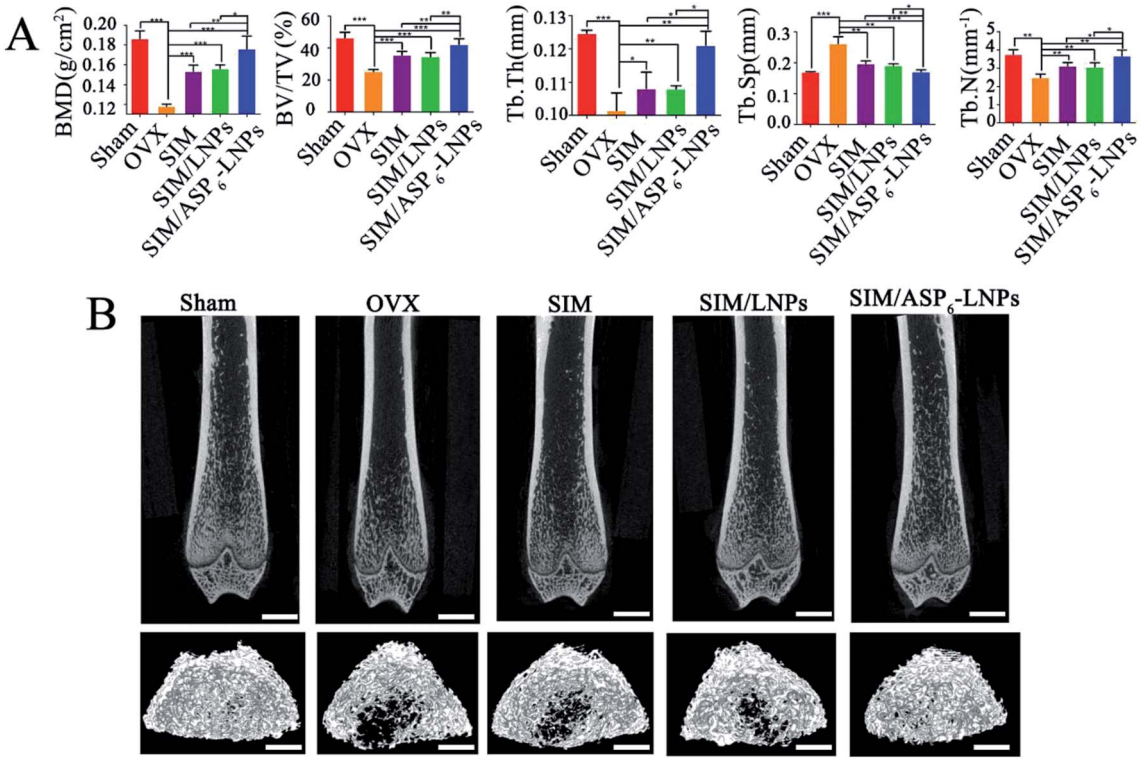

Fig. 8 Micro-CT analysis of bone tissue in rats. (A) The trabecular bone density (BMD), trabecular bone volume percentage (BV/TV), trabecular separation (Tb. Sp), trabecular thickness (Tb. Th) and trabecular number (Tb. N) of the femur in all experimental groups. Average values of Sham, SIM, SIM/LNPs and SIM/ASP_6-LNPs were higher than that of OVX group during 12 weeks, and the difference was statistically significant. (B) 2D and 3D images of trabecular bone measured by micro-CT, indicating a gradually increase in microstructure and bone volume. Sham group was used as the positive control. The results represent the means ± SDs ($n = 3$), scale bar: 1 mm. *$p < 0.05$, **$p < 0.01$, ***$p < 0.001$.

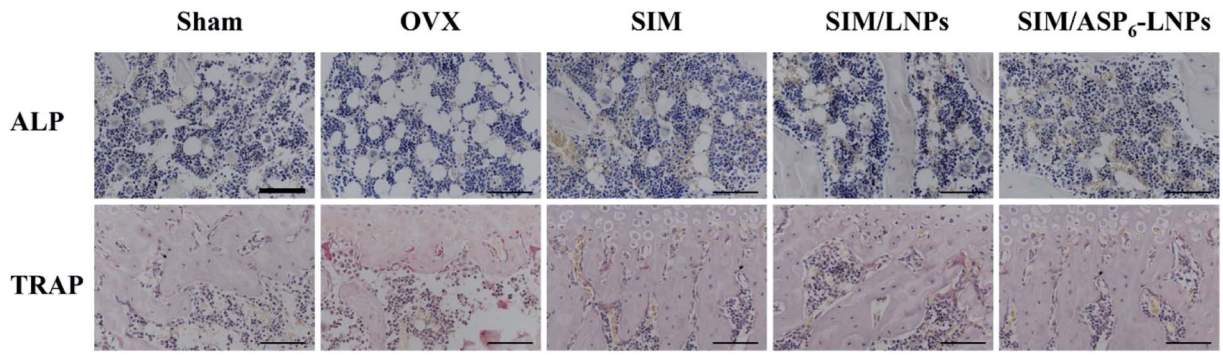

Fig. 9 Alkaline phosphatase (ALP) activity (arrows) and tartrate-resistant acid phosphatase (TRAP) assay results (arrowheads) of bone tissue sections. Scale bar = 50 μm. The ALP activity is much more high in SIM/LNPs and SIM/ASP_6-LNPs groups, while the TRAP activity is the opposite.

indicating a significant improvement in microstructure and bone volume.

2.5.3.3 Alkaline phosphatase (ALP) activity and tartrate-resistant acid phosphatase (TRAP) assay. During the process of SIM augmentation of BMP-2-induced osteoblast differentiation, Runx2 expression and ALP activity increases through the BMP-Smad signaling pathway. As shown in Fig. 9, in the experimental groups, the activity of ALP was higher than that of the OVX group. As we can see, in the figure, several cells are brought together, and the surrounding gray area is the newly formed bone matrix, indicating that new bone is forming. In these areas, the activity of ALP is high. In the OVX groups, ALP activity was relatively low. In contrast, TRAP activity is relatively high, indicating that osteoblast activity is stronger than osteoclast activity. In addition, the modification of ASP_6 can increase the distribution of SIM/ASP_6-LNPs in the bone and increase the concentration of SIM at the bone site. Therefore, the ALP activity of the SIM/ASP_6-LNPs groups was the highest and almost the same as that of the SHAM group. Meanwhile, the TRAP activity of SIM/ASP_6-LNPs is as low as that of the SHAM group.

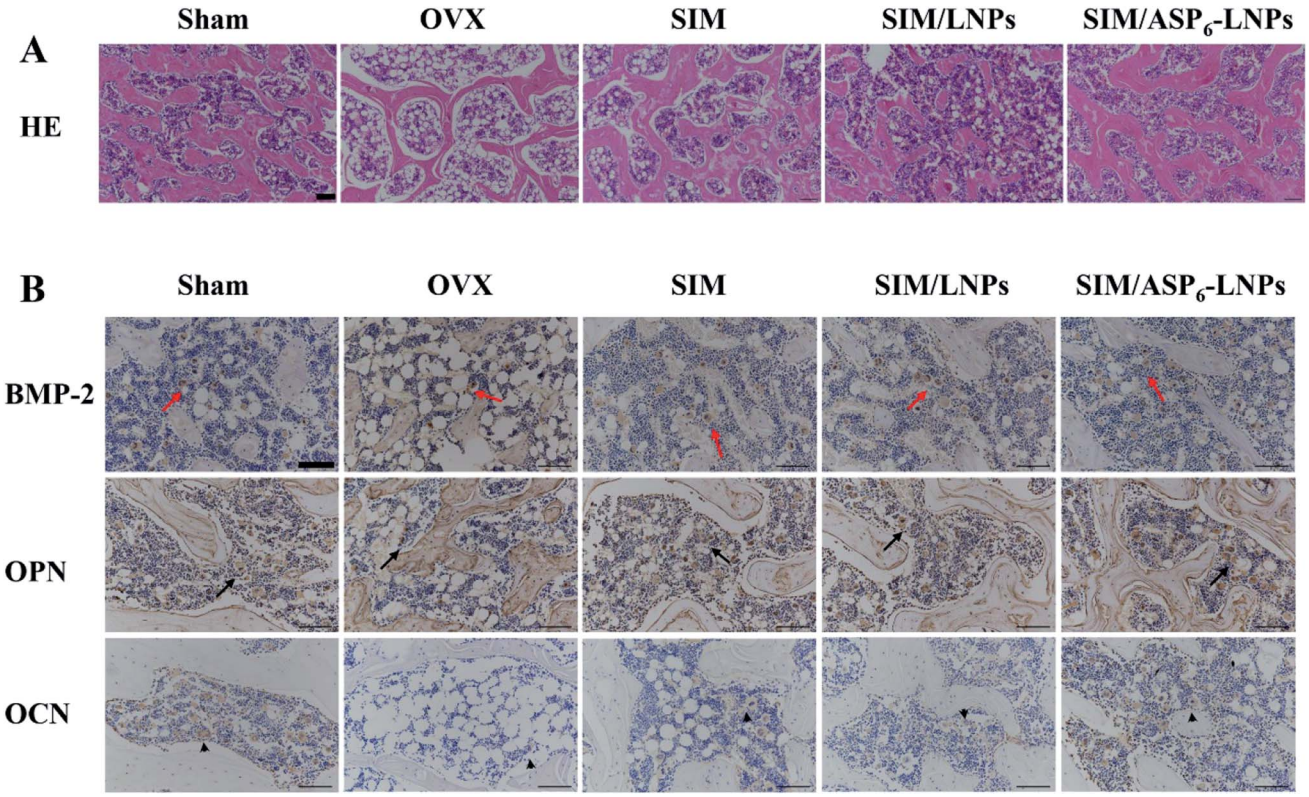

Fig. 10 Histological assessment of bone formation in all experimental groups. (A) H&E staining of femur bone. Scale bar = 50 μm. Histology of bone in the all experimental groups shows all ovariectomized groups had a higher amount of adipose tissue than Sham group. The trabecular bone is much more prominent in SIM/LNPs and SIM/ASP_6-LNPs groups. (B) Immunohistochemical staining for BMP-2 in typical newly-formed bone tissue (red arrows) and immunohistochemical staining for the osteogenic markers osteopontin (OPN, arrows) and osteocalcin (OCN, arrowheads). Scale bar = 50 μm. The BMP-2, OPN, OCN are much more prominent in SIM/LNPs and SIM/ASP_6-LNPs groups.

2.5.3.4 Histological analysis and immunohistochemistry (IHC). All sections of femurs were evaluated histologically (Fig. 10A). Because SIM has the potential to promote new bone formation, normal compactness of the femur and competent trabeculae were observed in the Sham group, while the OVX group showed sparse loss of interconnectivity and thinning of the trabeculae, thereby showing widened intertrabecular spaces. The OVX group showed more adipose tissue than the other groups did. There was a statistically significant increase in trabecular interconnectivity in the SIM-, SIM/LNPs- and SIM/ASP_6-LNPs-treated groups in comparison to the OVX group. The trabecular bone is much more prominent in the SIM/ASP_6-LNPs group due to the bone-targeting ability of ASP_6, thus increasing the accumulation of SIM in bones and increasing the drug efficacy. It is gratifying that the SIM/ASP_6-LNPs-treated group showed more resemblance to the Sham group. Overall, the bone histological analysis indicated a marked recovery effect of SIM and showed a restored architecture with this treatment regime in the ovariectomy-induced osteoporosis model in rats.

The results of IHC staining are shown in Fig. 10B. SIM can promote the differentiation and mineralization of osteoblasts through the BMP-Smad signaling pathway; therefore, we can study the efficacy of SIM by studying the expression of BMP-2 protein and the mineralization markers OPN and OCN. We found that BMP-2 and the osteogenic markers OPN and OCN were highly expressed in both the SIM/LNPs and SIM/ASP_6-LNPs groups. Moreover, the SIM/ASP_6-LNPs group showed higher expression of BMP-2, osteopontin (OPN) and osteocalcin (OCN) than that in the SIM/LNPs group due to the bone-targeting ability of ASP_6, indicating that SIM can induce osteoblastic differentiation through the BMP-Smad signaling pathway and that the nanocarrier SIM/ASP_6-LNPs we built can transport more SIM to the bone to better treat osteoporosis.

3. Conclusion

In this study, we designed and prepared a novel therapeutic agent to prevent and treat osteoporosis, which is composed of lipid material serving as a core and a drug pocket, SIM serving as an anti-osteoporosis drug and ASP_6 as a bone-targeting moiety. The results indicated that SIM/ASP_6-LNPs showed good entrapment of SIM and exhibited a sustained release of 70% within 48 hours. *In vivo* experiments described that the ASP_6-LNPs had an ideal bone-targeting ability in ICR mice, and *in vitro* cell experiments revealed that the LNPs had a great capacity for cell uptake and excellent biocompatibility with MC3T3-E1 cells, thus reducing the cytotoxicity of SIM. In addition, the cell mineralization assay suggested that the SIM/LNPs induced osteoblast differentiation and mineralization as well as the formation of mineralized nodules, achieving the same

efficacy as SIM though augmenting the BMP-Smad signaling pathway. Animal pharmacodynamics were performed in rats that underwent bilateral ovariectomies, and the results indicated that the SIM/ASP_6-LNPs can significantly improve the efficacy of SIM on the recovery of bone mineral density when compared with either SIM/LNPs or SIM alone. Therefore, ASP_6-LNPs may represent a potential bone-targeting drug delivery system (DDS), contributing to a novel osteoporosis therapy by SIM. This study is the first to employ LNPs to deliver SIM with ASP_6 grafted as a biocompatible bone-targeting moiety for osteoporosis therapy in an *in vivo* model, which opens up a new avenue for the treatment of osteoporosis.

4. Materials and methods

4.1 Materials

Monostearin and hydroxyapatite powder (HAP) was obtained from Shanghai Chemical Reagent Co., Ltd. (Shanghai, China). Polyethylene glycol monostearate (PEG_{2000}-SA, MW = 2000) was purchased from Tokyo Kasei Kogyo Co., Ltd. (Tokyo, Japan). Amino-terminated polyethylene glycol (NH_2-PEG_{2000}-NH_2, MW = 2000) was purchased from Yare Biotech, Inc. (Shanghai, China). SIM was from Zhejiang Hisun Pharmaceutical Co., Ltd. (Zhejiang, China). Aspartic oligopeptides (ASP_6) were purchased from Synpeptide Co., Ltd. (Shanghai, China). Octadecylamine (ODA), 4′,6-diamidino-2-phenylindole (DAPI), fluorescein isothiocyanate (FITC), stearic acid (SA), *N*,*N*′-disuccinimidyl carbonate (DSC), 1-(3-dimethylaminopropyl)-3-ethylcarbodiimide (EDC), *N*-hydroxysuccinimide (NHS), L-ascorbic acid, alizarin red S, β-glycerophosphate and 3-(4,5-dimethylthiazol-2-yl)-2,5-diphenyltetrazolium bromide (MTT) were obtained from Sigma Chemical Co. (St. Louis, MO, USA). Poloxamer 188 was obtained from Shenyang Jiqi Pharmaceutical Co., Ltd. (China). The bicinchoninic acid (BCA) protein assay kit and ALP test kit were obtained from the Beyotime Institute of Biotechnology (Haimen, Jiangsu, People's Republic of China). Iodide (DiR) lipophilic fluorescent dye was purchased from Molecular Probes (Eugene, OR, USA). Alpha-minimum essential medium (αMEM) was from Thermo Fisher Scientific (Waltham, MA, USA). Other reagents were analytical or chromatographic grade.

4.2 Methods

4.2.1 Synthesis and characterization of amino-terminated polyethylene glycol monostearate (NH_2-PEG_{2000}-SA). Under the catalytic conditions of EDC and NHS, we obtained NH_2-PEG_{2000}-SA by grafting the amine group of NH_2-PEG_{2000}-NH_2 with the carboxyl group of SA. Briefly, 34.2 mg of SA, 69 mg of EDC and 41.4 mg of NHS (SA : EDC : NHS = 1 : 3 : 3) were codissolved in 4 mL of anhydrous dimethyl sulfoxide (DMSO), and the carboxyl group was activated under mechanical stirring at 400 rpm and 60 °C for 30 min. The reaction solution was then added dropwise to 6 mL of anhydrous DMSO containing 240 mg of NH_2-PEG_{2000}-NH_2 (SA : NH_2-PEG_{2000}-NH_2 = 1 : 1, mol mol^{-1}). After 24 h of reaction under stirring at room temperature, NH_2-PEG_{2000}-SA was obtained, which was then dialyzed against distilled water for 48 h using a dialysis membrane bag (molecular cutoff = 7 kDa). The product was finally lyophilized and stored for further use at −20 °C. The structure of NH_2-PEG_{2000}-SA was subsequently evaluated by ^{1}H NMR, IR spectroscopy, ^{1}C NMR spectra and mass spectrum.

4.2.2 Preparation of fluorescent label ODA-FITC. We synthesized the fluorescent label ODA-FITC by chemical grafting between the amino group of ODA and the isothiocyanate group of FITC. Briefly, we dissolved 28 mg of FITC and 20 mg of ODA in 6 mL of ethanol and stirred the mixture at 50 °C for 24 h in the dark. After the reaction was complete, 50 mL of distilled water was added to the mixed solution to precipitate ODA-FITC. Subsequently, we isolated the product with a filter and washed the product three times using distilled water. Finally, we dried ODA-FITC at room temperature and stored it in the dark for further use.

4.2.3 Preparation of blank LNPs and SIM-loaded LNPs (SIM/LNPs). We prepared blank LNPs using the solvent diffusion method. Briefly, 8 mg of monostearin, 1 mg of polyethylene glycol monostearate (PEG_{2000}-SA), 1 mg of NH_2-PEG_{2000}-SA and 2 mg of oleic acid (OA) were codissolved in 1 mL of ethanol and heated to 70 °C. Then, under mechanical stirring at 400 rpm, the organic phase was quickly injected into 9 mL of 70 °C deionized water (ethanol : water = 1 : 9, v/v). After stirring for 5 min, the solution was cooled at room temperature to obtain blank LNPs (1 mg mL^{-1}). When preparing SIM/LNPs, 8 mg of monostearin, 1 mg of PEG_{2000}-SA, 1 mg of NH_2-PEG_{2000}-SA, 2 mg of oleic acid (OA) and 0.5 mg of SIM were codissolved in 1 mL of ethanol and heated to 70 °C. Then, under mechanical stirring at 400 rpm, the organic phase was quickly injected into 9 mL of 70 °C deionized water (ethanol : water = 1 : 9, v/v). After stirring for 5 min, the solution was cooled at room temperature to obtain SIM/LNPs.

4.2.4 Preparation and composition analysis of ASP_6-conjugated LNPs (ASP_6-LNPs). ASP_6-conjugated LNPs (ASP_6-LNPs) were prepared according to previous reports.[31,32] First, 10 mL of blank LNPs were obtained with the aforementioned method. Then, 226 μL of a 0.5 mg mL^{-1} DSC aqueous solution (NH_2-PEG_{2000}-SA : DSC = 1 : 1, mol mol^{-1}) was added to the LNPs, stirred at room temperature for 3 h, and then 78 μL of a 4 mg mL^{-1} aqueous solution of Asp_6 was added thereto (NH_2-PEG_{2000}-SA : ASP_6 = 1 : 1, mol mol^{-1}) and stirred at room temperature for 3 hours. ASP_6-conjugated LNPs were prepared. An elemental analyzer method (vario MICRO cube, Elementar Analysensysteme GmbH) confirmed whether ASP_6 was conjugated successfully by analyzing the nitrogen content of LNPs and ASP_6-LNPs. The preparation of ASP_6-conjugated SIM/LNPs (SIM/ASP_6-LNPs) was similar to that of ASP_6-LNPs, adding 0.5 mg of SIM to the lipid ingredients.

4.2.5 Physical characterization of LNPs and evaluation of SIM/LNPs

4.2.5.1 Size, zeta potential and morphology measurements. First, the carrier concentrations of LNPs and SIM/LNPs were diluted to 100 μg mL^{-1} using distilled water. Then, the hydrodynamic diameter, polydispersity index (PI) and zeta potential of LNPs and SIM/LNPs were measured by DLS using a Zetasizer (3000HS, Malvern Instruments Ltd., UK), followed by TEM (JEM1230, JEOL, Japan) for morphological examination. Briefly,

the samples were placed on a copper mesh and air dried naturally, and then negatively stained with 1% (w/v) uranyl acetate for TEM.

4.2.5.2 Drug encapsulation efficiency and drug loading content. The concentration of SIM in LNPs and ASP_6-LNPs was analyzed by a high-performance liquid chromatography (HPLC), system using an Agilent ZORBAX SB-C18 column (4.6 mm × 150 mm, 5 μm). The mobile phase is 25 mM aqueous solution of sodium dihydrogen phosphate–acetonitrile (35 : 65, v : v).The constant flow rate was 1 mL min^{-1}, and the wavelength of ultraviolet detection was 239 nm. In addition, the column temperature was 35 °C. The retention time is 9.8 min and injection volume was 100 μL. The standard curve was used to determine the content of SIM through external standard method. The standard curve was prepared as follows: 10 mg of SIM was weighed accurately and placed in a 10 mL volumetric flask, after which ethanol was added to the volumetric flask up to the mark to obtain 1.0 mg mL^{-1} SIM ethanol solution, then pipette the appropriate amount of the above simvastatin ethanol solution accurately with a pipette and dilute with mobile phase to 1 μg mL^{-1}, 2 μg mL^{-1}, 5 μg mL^{-1}, 10 μg mL^{-1} and 20 μg mL^{-1}. The peak area of the chromatogram was detected by HPLC, and the standard area was plotted with the peak area S plotted against the concentration of simvastatin C (μg mL^{-1}). The results show that the standard curve of SIM is $y = 287.47 \times 53.604$, the correlation coefficient $R^2 = 1$, the linear range is 1–20 μg mL^{-1}, and the linear relationship meets the content determination requirements.

First, the formulated SIM/LNPs and SIM/ASP_6-LNPs dispersions were flocculated by adding 1 M hydrochloric acid (HCl) until the pH value of the dispersions was 1.2. Then, SIM/LNPs and SIM/ASP_6-LNPs were separated by centrifugation at 20 000 rpm for 15 min (3K30, Sigma Labrorzentrifugen GmbH, Germany). The concentration of free SIM in the supernatant was measured, and the separated precipitate was redispersed with 15 mL of PBS (pH 7.4). The redispersed dispersions were vortexed for 3 min to dissolve the drug adsorbed on the surface of the LNPs and ASP_6-LNPs. The dispersions were then centrifuged at 20 000 rpm for 15 min (3K30, Sigma, Germany). The supernatant was obtained, and the content of SIM therein was measured through HPLC. Finally, we calculated the EE% and DL% of SIM in LNPs using the following formulas:

$$EE\% = (W_0 - W_a - W_b)/W_0 \times 100\%$$

$$DL\% = (W_0 - W_a - W_b)/(W_0 - W_a - W_b + W) \times 100\%$$

W_0 is the total weight of drugs added to the system, W_a represents the weight of free drug in the supernatant after the first centrifugation, W_b is the weight of drug in the supernatant after the second centrifugation and W represents total weight of lipid material added to the system.

4.2.5.3 In vitro SIM release from SIM/LNPs and SIM/ASP_6-LNPs. In vitro release experiments were performed using a dialysis methods. Briefly, 15 mL of pH 7.4 phosphate buffered saline (PBS) was used as the release medium at 37 °C to mimic the physiological environment *in vivo*. One milliliter of SIM/LNPs and SIM/ASP_6-LNPs with a carrier concentration of 1 mg mL^{-1} were transferred to a dialysis bag with a molecular entrapment of 7 kDa, and the control group was a similar concentration of SIM in ethanol, subsequently the bags were immersed in PBS for release experiments using an incubator shaker. At the scheduled time point, we took 1 mL of medium and then added 1 mL of PBS. SIM released from SIM/LNPs and SIM/ASP_6-LNPs was quantified by HPLC. The standard curve was used to determine the content of SIM through external standard method.

4.2.6 Cell culture and evaluation

4.2.6.1 MC3T3-E1 cell culture. Clonal newborn mouse calvaria MC3T3-E1 cells were used as model cells to explore the behavior of LNPs in normal cells, which were cultured in alpha-minimum essential medium (αMEM) containing 10% (v/v) fetal bovine serum (FBS). When osteoblast differentiation and mineralization experiments were performed, 10 mmol L^{-1} β-glycerophosphate and 50 μg L^{-1} L-ascorbic acid were added to the basic medium. In addition, the cell culture medium was changed every other day.[33]

4.2.6.2 Cytotoxicity study. We evaluated the toxicity of the constructed nanocarriers to cells using the 3-(4,5-dimethylthiazol-2-yl)-2,5-diphenyltetrazolium bromide (MTT) method. MC3T3-E1 cells were seeded at 1×10^4 cells per well in 96-well plates and incubated for 24 h until they were attached to the wells, and then exposed to a series of concentrations of blank LNPs, SIM, SIM/LNPs and SIM/ASP_6-LNPs for 48 h, after which 20 μL of 5 mg mL^{-1} MTT was added to each well for another 4 h followed by adding 200 μL of DMSO into each well to dissolve the forming formazan crystals. Subsequently, these plates were shaken at 37 °C for 30 min, and the absorbance of each well at 570 nm was measured by an automatic microplate reader.

4.2.6.3 Cellular uptake of LNPs and ASP_6-LNPs. MC3T3-E1 cells were seeded at 1×10^5 cells per well in 12-well plates and incubated for 24 h until they were attached to the wells. Subsequently, cells were treated with fresh medium containing ODA-FITC-labeled LNPs and ASP_6-LNPs. To prepare the ODA-FITC-labeled LNPs and ASP_6-LNPs, ODA-FITC was added to equivalent lipid materials of the blank LNPs (ODA-FITC : lipid materials = 1 : 10, w/w). Then ODA-FITC-labeled LNPs and ASP_6-LNPs were prepared as mentioned above. At predetermined intervals (2, 4, 6, 10 h), the cells were collected and observed under a confocal microscope (Olympus, Japan). In addition, semiquantitative analysis of cellular uptake was assessed using flow cytometry.

4.2.6.4 Alizarin red S assay. MC3T3-E1 cells were seeded at 1×10^5 cells per well in 12-well plates and cultured in osteogenic differentiation and mineralization medium, which included SIM, SIM/LNPs and SIM/ASP_6-LNPs (the concentration of SIM was 10^{-7} mol L^{-1}) for 14 days. After 14 days of culture, the cells were fixed using 70% ethanol for 1 h, and subsequently stained with alizarin red S at a concentration of 1.5% at pH 4.0–4.2 for 10–15 min. Unreacted dye was removed and the formed mineralized nodules were observed under a light microscope. Finally, 10% cetylpyridinium chloride was added to each well to dissolve the alizarin red S in the cell matrix, and the

concentration of alizarin red S was calculated by measuring the UV absorbance of the sample at 562 nm.

4.2.6.5 Measurement of ALP activity. MC3T3-E1 cells were seeded at 1×10^5 cells per well in a 12-well plate and cultured in osteogenic differentiation and mineralization medium which includes SIM, SIM/LNPs and SIM/ASP_6-LNPs (the concentration of SIM was 10^{-7} mol L^{-1}) for 7 days. After 7 days of culture, the MC3T3-E1 cells were lysed with PBS with 0.1% Triton X-100 under ultrasound. Afterwards, ALP activity was measured using an ALP test kit.

4.2.7 *In vivo* testing

4.2.7.1 In vivo evaluation of the bone-targeting LNPs in mice. All animal procedures were performed in accordance with the Guidelines for Care and Use of Laboratory Animals of Zhejiang University and experiments were approved by the Animal Ethics Committee of Zhejiang University (China). The bone-targeting ability of LNPs and ASP_6-LNPs was evaluated in ICR mice. The lipophilic fluorescent dye DiR was used to detect LNPs and ASP_6-LNPs. Six ICR mice were randomly divided into two groups of three mice per group. A total of 0.2 mL of DiR-labeled LNPs and DiR-labeled ASP_6-LNPs (2 mg mL^{-1}) was tail-intravenously injected into mice. After 48 h, the mice were sacrificed, and their main organs (heart, liver, spleen, lungs, and kidneys) and the femur and tibia bones were obtained. The fluorescence signals in the main organs were subsequently detected with a Maestro EX *in vivo* imaging system. The fluorescence intensities were subsequently calculated as a percentage using the following equation:

$$\text{Distribution of fluorescence intensities } (\%) = \frac{A_{\text{tissue}}}{A_{5\%} \times 20} \times 100\%$$

A_{tissue} is the fluorescence intensity of the major organs, and $A_{5\%}$ is the fluorescence intensity of DiR-loaded LNPs at an injected dose of 5%.

4.2.7.2 Intrabone distribution of ODA-FITC-labeled LNPs and ASP_6-LNPs. First, ODA-FITC-labeled LNPs and ASP_6-LNPs were prepared. Xylenol orange was tail-intravenously injected into ICR mice to label the osteoid surfaces three days prior to injecting ODA-FITC-labeled LNPs and ASP_6-LNPs at a dose of 30 mg kg^{-1}.[30,34] ODA-FITC-labeled LNPs and ASP_6-LNPs were tail-intravenously injected into mice at a dose of 20 μmol FITC kg^{-1}. After 24 h, the mice were sacrificed and bones of the lower extremities were obtained. Undecalcified tissue sections of the distal femur and proximal tibia were generated using a previously reported method.[35] Afterwards, the sections were observed with a confocal microscope (Olympus, Japan).

4.2.7.3 Animal pharmacodynamics study. All animal studies were approved by the Committees of Animal Experiments at Zhejiang University in China. Female Sprague Dawley rats, which had a mean body weight of 180–200 g were housed in a climate-controlled environment with a 12/12 h light/dark cycle with access to standard food and water.

Twenty five female Sprague Dawley rats were randomly divided into five groups with five mice in each group: the Sham group, the OVX group, the SIM group with a dose of 1 mg per kg per 2 days, the SIM/LNPs group with a SIM dose of 1 mg per kg per 2 days and SIM/ASP_6-LNPs group with a SIM dose of 1 mg per kg per 2 days. All groups except the Sham group were all bilaterally ovariectomized, whereas the Sham group was subjected to a sham operation of intraperitoneal invasion. SIM, SIM/LNPs and SIM/ASP_6-LNPs were injected into rats starting 1 month after bilateral ovariectomy, and continuing for 2 months. The Sham and OVX groups were administered saline. After 2 months of administration, all animals were sacrificed. The main organs (heart, liver, spleen, lungs and kidneys) and the femurs of rats were obtained.

4.2.7.3.1 Histological analysis of excised organ samples. The excised organ samples (heart, liver, spleen, lungs and kidneys) of every animal were stained with H&E, after which they were observed under a light microscope (Nikon, ECLIPSE Ni).

4.2.7.3.2 Microcomputed tomography (micro-CT) and image analysis. Micro-CT was employed to analyze changes in the trabecular bone of the femur. A SkyScan-1176 (Bruker micro CT, Belgium) system (18 μm voxel size, 90 kV, 278 μA, 230 ms exposure time, Al 0.5 mm filter, 180° rotation step) was used for the examinations. The 1.6 version of NRecon software (Bruker micro CT, Belgium) was used for 3D reconstruction and viewing of images. After 3D reconstruction, the 1.13 version of CT software (Bruker micro CT, Belgium) was used for bone analysis. The index included bone mineral density (BMD), bone volume fraction (BV/TV), thickness (Tb. Th), number (Tb. N) and separation (Tb. Sp) were all calculated to evaluate the bone formed in the defect area.

4.2.7.3.3 Alkaline phosphatase (ALP) activity and tartrate-resistant acid phosphatase (TRAP) assay. As mentioned earlier, SIM has the potential to increase the activity of BMP-2 and promote the formation of new bone *in vitro* and in animals through the BMP-Smad signaling pathway. During this process, ALP activity increases and TRAP activity decreases. To evaluate the pharmacodynamic effect of SIM, all femurs were decalcified in ethylenediaminetetraacetic acid (EDTA), after which the femur were dehydrated and then embedded in paraffin. Then, sections (4 μm thickness) were stained with ALP and TRAP.

4.2.7.3.4 Histological analysis and immunohistochemistry. All femurs were decalcified in EDTA, dehydrated, and then embedded in paraffin to obtain sections of 4 μm thickness, which were then stained with hematoxylin and eosin (H&E). In addition, the osteogenic effects of SIM were assessed by immunohistochemistry (IHC) analysis of osteopontin (OPN) and osteocalcin (OCN). To further explore the mechanism of bone formation, IHC staining of BMP-2 was also performed.

4.3 Statistical analysis

The results are expressed as the means ± standard deviations (SDs) unless noted otherwise. The statistical analyses of the data were performed using Student's *t*-test. Differences characterized by $P < 0.05$ were considered statistically significant.

Conflicts of interest

There are no conflicts of interest to declare.

Acknowledgements

This research was supported by Zhejiang Natural Science Foundation (LY18H060002), Project of Health Commission of Zhejiang Province (2016KYA115) and the National Natural Science Foundation of China under Contract No. 81573366, 81773644.

References

1 D. N. Heo, W. K. Ko, H. J. Moon, H. J. Kim, S. J. Lee, J. B. Lee, M. S. Bae, J. K. Yi, Y. S. Hwang, J. B. Bang, *et al.*, Inhibition of osteoclast differentiation by gold nanoparticles functionalized with cyclodextrin curcumin complexes, *ACS Nano*, 2014, **8**(12), 12049–12062.

2 G. Mundy, R. Garrett, S. Harris, J. Chan, D. Chen, G. Rossini, B. Boyce, M. Zhao and G. Gutierrez, Stimulation of bone formation *in vitro* and in rodents by statins, *Science*, 1999, **286**(5446), 1946–1949.

3 M. Yamashita, F. Otsuka, T. Mukai, H. Otani, K. Inagaki, T. Miyoshi, J. Goto, M. Yamamura and H. Makino, Simvastatin antagonizes tumor necrosis factor-α inhibition of bone morphogenetic proteins-2-induced osteoblast differentiation by regulating Smad signaling and Ras/Rho-mitogen-activated protein kinase pathway, *J. Endocrinol.*, 2008, **196**(3), 601–613.

4 C. B. Blum, Comparison of properties of four inhibitors of 3-hdroxy-3meth-yglutary-coenzyme A reductase, *Am. J. Cardiol.*, 1994, **73**, 3D–11D.

5 A. Montagnani, S. Gonnelli, C. Cepollaro, S. Pacini, M. S. Campagna, M. B. Franci, B. Lucani and C. Genari, Effect of simvastatin treatment on bone mineral density and bone turnover in hypercholesterolemic postmenopausal women: a 1-year longitudinal study, *Bone*, 2003, **32**, 427–433.

6 C. Tikiz, H. Tikiz, F. Taneli, G. Gumuser and C. Tuzun, Effects of simvastatin on bone mineral density and remodeling parameters in postmenopausal osteopenic subjects: 1-year follow-up study, *Clin. Rheumatol.*, 2005, **24**, 447–452.

7 H. Wang, J. Liu, S. Tao, G. H. Chai, J. W. Wang, F. Q. Hu and H. Yuan, Tetracycline-grafted PLGA nanoparticles as bone-targeting drug delivery system, *Int. J. Nanomed.*, 2015, **10**, 5671.

8 Z. Z. Zhang, H. Z. Zhang and Z. Y. Zhang, 3D printed poly (ε-caprolactone) scaffolds function with simvastatin-loaded poly (lactic-*co*-glycolic acid) microspheres to repair load-bearing segmental bone defects, *Exp. Ther. Med.*, 2019, **17**(1), 79–90.

9 W. L. Yu, T. W. Sun and C. Qi, Enhanced osteogenesis and angiogenesis by mesoporous hydroxyapatite microspheres-derived simvastatin sustained release system for superior bone regeneration, *Sci. Rep.*, 2017, **7**, 44129.

10 W. Mehnert and K. Mäder, Solid lipid nanoparticles: production, characterization and applications, *Adv. Drug Delivery Rev.*, 2012, **64**, 83–101.

11 J. Wang, J. Chen, N. S. Ye, Z. Q. Luo, W. L. Lai, X. X. Cai and Y. F. Lin, Absorption, pharmacokinetics and disposition properties of solid lipid nanoparticles (SLNs), *Curr. Drug Metab.*, 2012, **13**(4), 447–456.

12 Y. J. Zhai and G. X. Zhai, Advances in lipid-based colloid systems as drug carrier for topic delivery, *J. Controlled Release*, 2014, **193**, 90–99.

13 Q. Yu, X. W. Hu, Y. H. Ma, Y. C. Xie, Y. Lu, J. P. Qi, L. Xiang, F. Q. Li and W. Wu, Lipids-based nanostructured lipid carriers (NLCs) for improved oral bioavailability of sirolimus, *Drug Delivery*, 2016, **23**(4), 1469–1475.

14 X. Yue, M. Niu and T. Zhang, *In vivo* evaluation of a simvastatin-loaded nanostructured lipid carrier for bone tissue regeneration, *Nanotechnology*, 2016, **27**(11), 115708.

15 S. A. Low and J. Kopeček, Targeting polymer therapeutics to bone, *Adv. Drug Delivery Rev.*, 2012, **64**(12), 1189–1204.

16 D. Wang, S. C. Miller, P. Kopečková and J. Kopeček, Bone-targeting macromolecular therapeutics, *Adv. Drug Delivery Rev.*, 2005, **57**, 1049–1076.

17 W. L. Ye, Y. P. Zhao, R. Na, F. Li, Q. B. Mei, M. G. Zhao and S. Y. Zhou, Actively targeted delivery of doxorubicin to bone metastases by a pH-sensitive conjugation, *J. Pharm. Sci.*, 2015, **104**(7), 2293–2303.

18 M. McClung, S. T. Harris, P. D. Miller, D. C. Bauer, K. S. Davison, L. D. MB, D. A. Hanley, D. L. Kendler, C. K. Yuen and E. M. Lewiecki, Bisphosphonate therapy for osteoporosis: benefits, risks, and drug holiday, *Am. J. Med.*, 2013, **126**(1), 13–20.

19 V. Vennila, V. Madhu, R. Rajesh, K. K. R. Ealla, S. R. Velidandla and S. Santoshi, Tetracycline-induced discoloration of deciduous teeth: case series, *J. Int. Oral Health*, 2014, **6**(3), 115.

20 S. Kasugai, R. Fujisawa, Y. Waki, K. I. Miyamoto and K. Ohya, Selective drug delivery system to bone: small peptide (Asp) 6 conjugation, *J. Bone Miner. Res.*, 2000, **15**(5), 936–943.

21 D. K. Yarbrough, E. Hagerman, R. Eckert, J. He, H. Choi, N. Cao, K. Le, J. Hedger, F. Qi, M. Anderson, *et al.*, Specific binding and mineralization of calcified surfaces by small peptides, *Calcif. Tissue Int.*, 2010, **86**(1), 58–66.

22 M. B. Murphy, J. D. Hartgerink, A. Goepferich and A. G. Mikos, Synthesis and *in vitro* hydroxyapatite binding of peptides conjugated to calcium-binding moieties, *Biomacromolecules*, 2007, **8**(7), 2237–2243.

23 S. A. Low and J. Kopeček, Targeting polymer therapeutics to bone, *Adv. Drug Delivery Rev.*, 2012, **64**, 1189–1204.

24 T. Sekido, N. Sakura, Y. Higashi, K. Miya, Y. Nitta, M. Nomura, H. Sawanishi, K. Morito, Y. Masamune and S. Kasugai, Novel drug delivery system to bone using acidic oligopeptide: pharmacokinetic characteristics and pharmacological potential, *J. Drug Targeting*, 2001, **9**, 111–121.

25 M. Ansar, D. Serrano, I. Papademetriou, T. K. Bhowmick and S. Muro, Biological functionalization of drug delivery carriers to bypass size restrictions of receptor-mediated endocytosis independently from receptor targeting, *ACS Nano*, 2013, **7**(12), 10597–10611.

26 C. A. Gregory, W. G. Gunn, A. Peister and D. J. Prockop, An Alizarin red-based assay of mineralization by adherent cells in culture: comparison with cetylpyridinium chloride extraction, *Anal. Biochem.*, 2004, **329**(1), 77–84.

27 T. Maeda, A. Matsunuma, T. Kawane and N. Horiuchi, Simvastatin promotes osteoblast differentiation and mineralization in MC3T3-E1 cells, *Biochem. Biophys. Res. Commun.*, 2001, **280**(3), 874–877.

28 T. Maeda, A. Matsunuma, I. Kurahashi, T. Yanagawa, H. Yoshida and N. Horiuchi, Induction of osteoblast differentiation indices by statins in MC3T3-E1 cells, *J. Cell. Biochem.*, 2004, **92**(3), 458–471.

29 L. Wong, R. Bendayan, A. M. Rauth, Y. Q. Li and X. Y. Wu, Chemotherapy with anticancer drugs encapsulated in solid lipid nanoparticles, *Adv. Drug Delivery Rev.*, 2007, **59**(6), 491–504.

30 G. Zhang, B. S. Guo, H. Wu, T. Tang, B. T. Zhang, L. Z. Zheng, Y. X. He, Z. J. Yang, X. H. Pan and H. Chow, A delivery system targeting bone formation surfaces to facilitate RNAi-based anabolic therapy, *Nat. Med.*, 2012, **18**, 307–314.

31 Y. M. Lu, J. Y. Huang, H. Wang, X. F. Lou, M. H. Liao, L. J. Hong, R. R. Tao, M. M. Ahmed, C. L. Shan and X. L. Wang, Targeted therapy of brain ischaemia using Fas ligand antibody conjugated PEG-lipid nanoparticles, *Biomaterials*, 2014, **35**(1), 530–537.

32 S. J. Li, X. J. Wang, J. B. Hu, X. Q. Kang, L. Chen, X. L. Xu, X. Y. Ying, S. P. Jiang and Y. Z. Du, Targeting delivery of simvastatin using ICAM-1 antibody-conjugated nanostructured lipid carriers for acute lung injury therapy, *Drug Delivery*, 2017, **24**(1), 402–413.

33 F. Yang, S. Zhao, F. Zhang, F. M. He and G. L. Yang, Simvastatin-loaded porous implant surfaces stimulate preosteoblasts differentiation: an *in vitro* study, *Oral Surgery, Oral Medicine, Oral Pathology, Oral Radiology, and Endodontology*, 2011, **111**(5), 551–556.

34 M. Hirose, N. Kotobuki, H. Machida, E. Uchimura and H. Ohgushi, Quantitative monitoring of *in vitro* mineralization process using fluorescent dyes, *Key Eng. Mater.*, 2003, **240**, 715–718.

35 T. Kawamoto, Use of a new adhesive film for the preparation of multi-purpose freshfrozen sections from hard tissues, whole-animals, insects, and plants, *Arch. Histol. Cytol.*, 2003, **66**, 123–143.